SEISMIC ANISOTROPY IN SALT STRUCTURES DUE TO PREFERRED CRYSTAL ORIENTATION

D. G. RAYMER and J. M. KENDALL

School of Earth Sciences[1]

ANISOTROPIE SISMIQUE DANS LES STRUCTURES SALIFÈRES DUE À L'ORIENTATION PRÉFÉRENTIELLE DES CRISTAUX

L'analyse de la texture du sel gemme naturel et du halite déformé expérimentalement a montré qu'il se produit une orientation préférentielle du réseau dans les cristaux de halite. Les paramètres d'élasticité pour une série d'agrégats polycristallins de halite sont calculés en utilisant les fonctions de distribution d'orientation. Ils sont alors utilisés pour élaborer des modèles sismiques dans lesquels sont tracés des rayons afin d'étudier les effets potentiels de l'anisotropie sismique dans les structures salifères. Les modèles salifères anisotropes montrent une variation significative dans le temps de propagation par rapport au modèle salifère isotrope, et un effet important de biréfringence des ondes transversales est prédit.

SEISMIC ANISOTROPY IN SALT STRUCTURES DUE TO PREFERRED CRYSTAL ORIENTATION

Texture analysis of natural rock salt and experimentally deformed halite have shown that lattice preferred orientation of halite crystals does occur. The elastic parameters for a range of halite polycrystalline aggregates are calculated using orientation distribution functions. These are used to construct seismic models which are ray-traced through to investigate the potential effects of seismic anisotropy in salt structures. Anisotropic salt models show significant variation in travel time from the isotropic salt model and large shear-wave splitting is predicted.

ANISOTROPÍA SÍSMICA EN ESTRUCTURAS SALINAS CAUSADA POR ORIENTACIÓN PREFERENCIAL DE LOS CRISTALES

El análisis de la textura de la roca salina natural y de la halita experimentalmente deformada demuestra que se produce una orientación reticular preferencial en los cristales de halita. Los parámetros elásticos de una serie de agregados policristalinos de halita se calculan utilizando funciones de distribución de la orientación. Estas funciones se utilizan para construir modelos sísmicos que son atravesados por trazados de rayos con el fin de

(1) University of Leeds,
Leeds LS2 9JT - United Kingdom

investigar los efectos potenciales de la anisotropía sísmica sobre las estructuras salinas. Los modelos salinos anisotrópicos muestran una variación significativa del tiempo de desplazamiento con respecto al modelo salino isotrópico y se predice una amplia división por onda de cizallamiento.

INTRODUCTION

The interpretation of seismic data from salt environments is important in locating hydrocarbon reserves found next to salt structures and in sub-salt locations. Errors in interpretation discovered at the drilling stage can be costly so greater understanding of the seismic problems associated with salt are of interest. The errors are generally attributed to the structural complexity, which is due to the fact that salt flows quite easily in response to tectonic forces, and large velocity contrasts associated with salt.

The density of halite is effectively invariant with depth of burial leading to large density contrasts between the salt and surrounding rocks. This density contrast, and the fact that evaporites deform more readily than other consolidated sediments, can lead to the flow of salt to form structures such as diapirs and sills. Salt tectonics is the field of study which explains how the salt forms such structures and surrounding lithology is deformed (Jackson *et al.*, 1994; Jenyon, 1986).

The deformation of salt during flow can lead to lattice preferred orientation of the constituent crystals. Halite (NaCl) is the main constituent of many salt bodies. Although optically isotropic, halite crystals are elastically anisotropic with single crystal seismic anisotropies of 7.0% and 16.4% for the *P*- and *S*-waves respectively (Fig. 1). As single halite crystals are anisotropic any lattice preferred orientation will lead to an effective anisotropy of the deformed polycrystalline aggregate. If the type of deformation occurring in the salt body is similar over a large area the lattice preferred orientation may lead to significant seismic effects.

The deformation that occurs during the creation and evolution of salt bodies is dependent on many factors such as the flow geometry and velocity, temperature and water content. The type and level of lattice preferred orientation are determined by these factors. In this paper we consider vertical flow in a 2-dimensional model of a salt diapir stem and investigate the consequences of the anisotropy due to lattice preferred orientation on the propagation of seismic waves through the model.

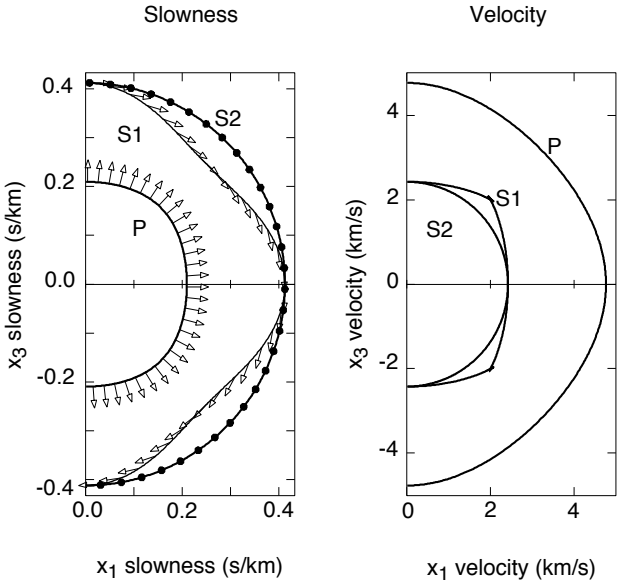

Figure 1

Vertical cross section of the slowness and velocity surfaces for single crystal halite. The plot on the left shows the slowness surfaces for the three body waves, the *P*-wave, the vertically polarized *S*-wave, *S*1 and the horizontally polarized *S*-wave, *S*2. The polarization directions are shown by the arrows with the filled circles indicating polarization straight out of the page. The plot on the right shows the velocity surfaces for these waves, the surfaces can be thought of as representing the shape of wave surfaces generated from a point source.

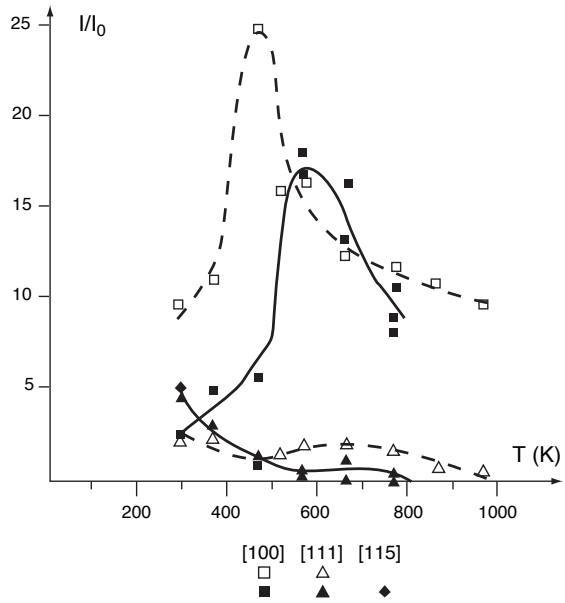

Figure 2

Temperature dependence of the maximum intensities of the preferred fibres in extruded synthetic (open) and natural salt (filled symbols). Intensities in units of random orientation distribution (from Skrotzki and Welch, 1983).

1 SALT DEFORMATION AND PREFERRED ORIENTATION

Lattice preferred orientation of halite crystals have been shown in texture analyses of experimentally and naturally deformed salt and by theoretical simulations of deformation. Halite deforms through slip on [110]<110>, [100]<110> and [111]<110> systems. In extrusion experiments carried out by Skrotzki and Welch (1983) on pure polycrystalline halite and natural rock salt, two main textures aligned with the extrusion axis. Generally the <111> axis and <100> axis align but the latter is replaced by <115> alignment at or below room temperatures in natural rock salt (Fig. 2). The <111> texture is due to lattice rotation during deformation by [110]<110> and [100]<110> slip and decreases with increasing temperature. The <100> texture is primarily due to dynamic recrystallisation and has a strong temperature dependence with a peak in texture intensity at ~600K for the natural rocksalt. This texture dominates above room temperature. They make an analogy between deformation by extrusion and that which occurs during diapirism. Other experimental deformation studies include shear and compression experiments (Franssen and Spiers, 1990) and triaxial deformation (Kern and Richter, 1985).

Some petrofabric analyses of naturally deformed salt in salt domes and other structures have been carried out. A sample from the Asse anticline in Germany (Kern and Richter, 1985) shows clear <100> alignment normal to the schistosity plane (Fig. 3a). Other studies include those of Schwerdtner (1968) (Fig. 3b), Muehlberger and Clabaugh (1968) (Fig. 3c) and Carter and Hansen (1983).

Theoretical simulations of halite deformation also provide information on the types and levels of anisotropy that can occur. There are a number of theoretical models for describing deformation, Wenk *et al.* (1989) compares texture development in halite using the Taylor theory and self-consistent theory.

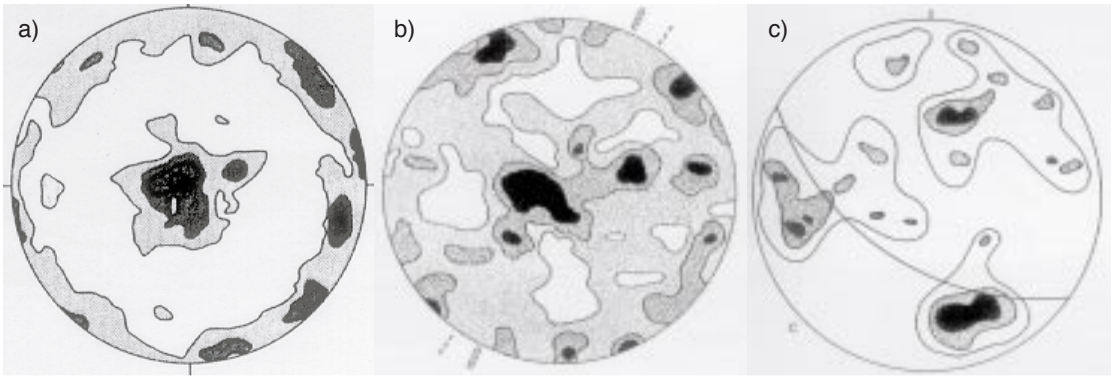

Figure 3

Examples of [100] pole figures for naturally deformed salt.
a) Rock salt from Asse anticline (Germany) plotted onto schistosity plane (Kern and Richter, 1985);
b) Specimen from Winnfield Salt Dome (Schwerdtner, 1968);
c) Specimen from Grand Saline Dome (Muehlberger and Clabaugh, 1968). Great circle indicates axial plane.

2 ORIENTATION DISTRIBUTION FUNCTION

The texture of a polycrystalline material can be described by a crystallite orientation distribution function. This gives the probability of an individual crystallite having a given orientation with respect to the sample axes. Knowledge of the distribution of the orientation of crystallites in a sample allows the aggregate elastic parameters of the sample to be calculated giving information about the seismic response of the sample.

To describe the orientation of a crystal within a sample two coordinate systems are required. One set of axes is fixed with respect to the sample, the other is fixed for a given crystal and for the case of cubic halite correspond to the [100], [010] and [001] crystallographic directions. The orientation of the crystal in respect to the sample is then uniquely defined by the three Euler angles ψ, θ and φ. The distribution of the crystal orientations within a sample is thus given by the crystallite orientation distribution function, w (ξ, ψ, φ) where = ξ cos (θ) (Sayers, 1982; Roe, 1965). This function gives the probability of finding a crystal with a given orientation, it clearly follows that:

$$\int_0^{2\pi}\int_0^{2\pi}\int_{-1}^{1} w(\xi,\psi,\varphi)\, d\xi\, d\psi\, d\varphi = 1 \qquad (1)$$

This can then be expanded into the form:

$$w(\xi,\psi,\varphi) = \sum_{l=0}^{\infty}\sum_{m=-l}^{l}\sum_{n=-l}^{l} w_{lmn}\, Z_{lmn}(\xi)\exp(-im\psi)\exp(-in\varphi) \qquad (2)$$

where Z_{lmn} are generalised Legendre functions defined in Roe (1965).

At this stage it is possible to obtain equations defining the stiffness tensor, C'_{ij}, of a sample. with orthorhombic symmetry. Here we consider the Voigt method which assumes uniformity of strain across grain boundaries and uses the stiffnesses. The derivation of these equations is given in Sayers (1982). The following calculations can also be done using compliances (Reuss) and combining both methods would allow the Voigt-Reuss-Hill average to be calculated (Allen *et al.* 1983).

For the case of a cubic crystal and assuming orthorhombic sample symmetry, C'_{ij}, is given in terms of the single crystal stiffness tensor, C_{ij} and the variables w_{400}, w_{440} and w_{420}.

Only the three w_{lmn} values are required due to the elastic parameters being completely described by terms of the w (ξ, ψ, φ) expansion with $l \leq 4$ (Sayers, 1982) and the consequences of symmetry (Roe, 1965; Roe, 1966).

For the case of transverse isotropy, where $w_{440} = w_{420} = 0$, the following equations are obtained:

$$
\begin{aligned}
C'_{11} &= C'_{22} = C_{11} - 2C\left\{\frac{1}{5} - \frac{6\sqrt{2}}{35}\pi^2 w_{400}\right\} \\
C'_{33} &= C_{11} - 2C\left\{\frac{1}{5} - \frac{16\sqrt{2}}{35}\pi^2 w_{400}\right\} \\
C'_{44} &= C'_{55} = C_{44} + C\left\{\frac{1}{5} - \frac{16\sqrt{2}}{35}\pi^2 w_{400}\right\} \\
C'_{66} &= C_{44} + C\left\{\frac{1}{5} + \frac{4\sqrt{2}}{35}\pi^2 w_{400}\right\} \\
C'_{23} &= C'_{13} = C_{12} + C\left\{\frac{1}{5} - \frac{16\sqrt{2}}{35}\pi^2 w_{400}\right\} \\
C'_{12} &= C_{12} + C\left\{\frac{1}{5} + \frac{4\sqrt{2}}{35}\pi^2 w_{400}\right\}
\end{aligned}
\tag{3}
$$

where $C = C_{11} - C_{12} - 2C_{44}$.

The plane-normal distribution, q (ζ, η), is the quantity that can be calculated from experimental texture analysis such as neutron diffraction. The term $\zeta = \cos\chi$ where χ is the polar angle and η is the azimuthal angle with respect to the sample coordinate system. The function q (ζ, η) can be expanded as a series of spherical harmonics and the coefficients of the series can be written in terms of w_{lmn}, so for the case of cubic crystals and an orthorhombic sample, q (ζ, η) can be defined in terms of w_{400}, w_{440} and w_{420} (Sayers, 1982):

$$
\begin{aligned}
4\pi q(\zeta,\eta) = 1 + 4\pi S\Bigg\{&\left(\frac{3}{8}\sqrt{2}\right)\left(35\zeta^4 - 30\zeta^2 + 3\right)w_{400} \\
&+ \frac{9}{2}\sqrt{5}\left(1-\zeta^2\right)\left[1 - \frac{7}{6}\left(1-\zeta^2\right)\right]w_{420} \\
&\cos 2\eta + \frac{3}{8}\sqrt{35}\left(1-\zeta^2\right)^2 w_{440}\cos 4\eta\Bigg\}
\end{aligned}
\tag{4}
$$

where S depends on which plane-normal the distribution is being calculated for.

The term $S = -\frac{4}{3}\pi$, 2π and $-\pi/2$ for the [111], [100] and [110] pole figures respectively.

The quantity $4\pi q$ (ζ, η) gives the degree of preferred alignment that occurs in a particular direction with $4\pi q$ (ζ, η) for random crystal alignment (Fig. 4).

Our work involves forward modelling, we assume a known value of w_{400} and calculate C'_{ij} and q (ζ, η). The orientation distribution function w (ξ, ψ, φ) can be calculated experimentally from C'_{ij} values which would be obtained from velocity measurements or from q (ζ, η) which can be obtained by texture analysis of the sample. If one of C'_{ij} and q (ζ, η) are known the other can be calculated by first calculating w (ξ, ψ, φ) as an intermediate stage.

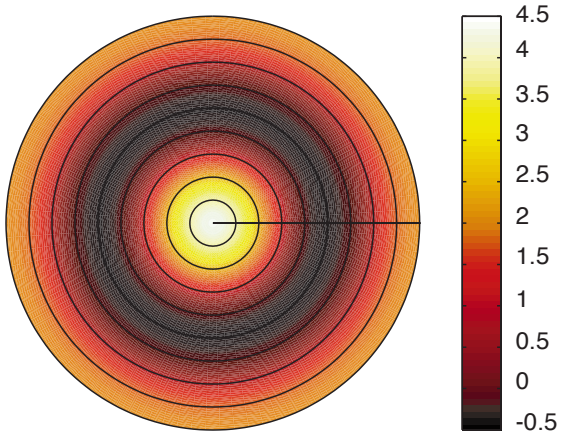

Figure 4

[100] pole figure for $w_{400} = 0.02$. The scale indicates the value of $4\pi q$ (ζ, η) with 1 representing a random distribution. This pole figure is the projection of $4\pi q$ (ζ, η) onto the x-y plane.

3 SEISMIC MODELLING

The model created is an idealised 2D representation of a stem of a salt diapir (Fig. 5). The diapir is assumed to consist of pure halite with a vertical flow direction surrounded by isotropic shale on each side. The deformation is considered as extrusion in the direction of flow which gives rise to lattice preferred orientation which is axially symmetric about the extrusion axis. This assumption means the salt is transversely isotropic so the type and intensity of preferred alignment depend only on the variable w_{400}.

This has the range of values $0.031345 \geq w_{400} \geq -0.020897$, the upper and lower limits representing perfect <100> and <111> alignment respectively and $w_{400} = 0$ represents an isotropic aggregate (Sayers, 1982).

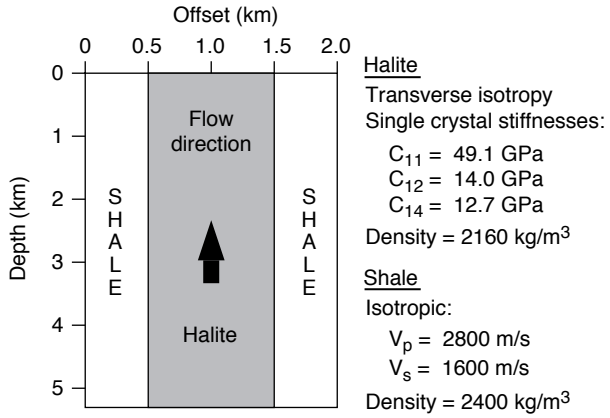

Figure 5

Geometry and physical parameters of the model created.

TABLE 1

w_{400} and anisotropy values of the halite in each model constructed

Model	w_{400}	Anisotropy (%)		Notes
		P-wave	*S*-wave	
A	0.031345	5.98	14.4	< 100 > alignment
B	0.02	3.85	9.18	
C	0.01	1.94	4.60	
D	0.00	0.00	0.00	isotropic aggregate
E	–0.007836	1.54	3.63	<110> alignment
F	–0.020897	4.15	9.78	<111> alignment

The three independent halite single crystal stiffnesses used were C_{11} = 49.1, C_{12} = 14.0 and C_{44} = 12.7 in units of GPa (Gebrande, 1982). Table 1 shows the models with varying w_{400} that were created and their respective anisotropies. Figure 4 shows the <100> pole figure created for w_{400} = 0.02, the symmetry about the extrusion axis is seen clearly.

For this situation q (ζ, η) is independent of the azimuth angle η so can be plotted just against χ. The cross-section through the plane-normal distributions for the [111], [100] and [110] crystallographic planes of each model are given in Figure 6. Negative values of $4\pi q$ (ζ, η) occur due to the truncation of the orientation distribution function expansion.

Although the elastic properties are described completely with $l \leq 4$, higher l values are required to give the true distribution of crystal orientations.

The models with w_{400} positive represent cases where the <100> alignment dominates as seen in the extrusion experiments of Skrotzki and Welch (1983) and in some observations of natural halite textures. When w_{400} is negative <111> or <110> alignment is dominating these types of alignment are seen in some types of deformation.

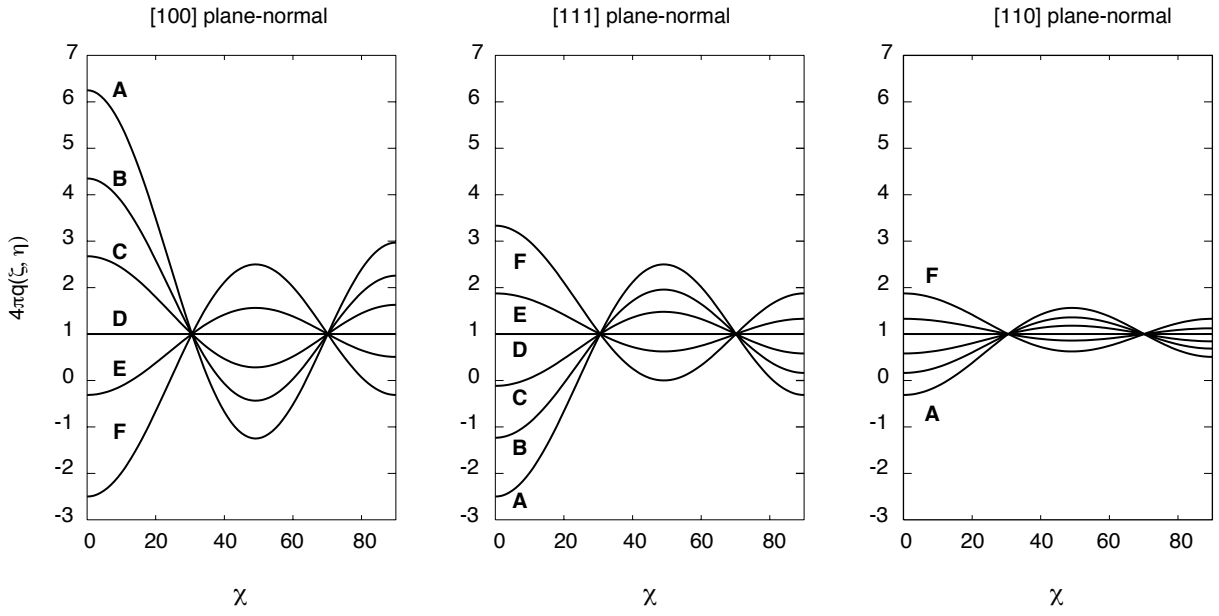

Figure 6

Cross-sections through $4\pi q$ (ζ, η), for all the models, for each of the [100], [111] and [110] plane normals.

4 RAY TRACING

The software package ATRAK which traces seismic rays in 3D, multi-layered, inhomogeneous, anisotropic media was used to create and ray trace through the models. The program is based on asymptotic ray theory (Guest and Kendall, 1993).

Rays were traced from an explosive source in the shale in the top left of the model, through the salt layer and to a vertical line in the shale at an offset of 2 km (Fig. 7). This configuration was chosen to represent a VSP scenario.

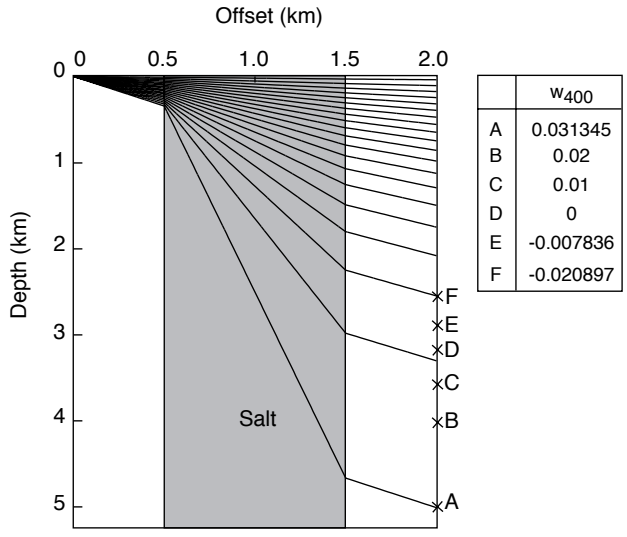

Figure 7

P-wave ray paths through the w_{400} = 0.031345 model. The crosses on the right indicate the arrival location of the ray with initial declination of 35.5° for each of the models.

P, *S*1 and *S*2-waves were traced for each model and the differences between travel times in the anisotropic and the isotropic salt models were calculated. The shear-wave splitting between the *S*1 and *S*2-waves was calculated for each model. The shear-waves were sorted by polarisation with *S*1 being the quasi-vertical wave and *S*2 the quasi-horizontal wave.

Ray-tracing was also used to investigate wave conversion at the salt-shale interfaces for an incoming *P*-wave. Due to the structure of the 2D model only conversions between *P* and *S*1-waves occur. If rays were traced in a plane which was not perpendicular to the interface, conversion between all three wave types would occur for the anisotropic models.

For the two extreme values of w_{400} and the isotropic case, four groups of rays were traced, *PPP*, *PPS*, *PSP* and *PSS*, where the three letters represent the wave type (*P*-wave and *S*1-wave) before entering the salt, in the salt and after leaving the salt respectively (Fig. 8). A comparison of travel times and amplitudes is made.

5 RESULTS

The marks labelled A-F in Figure 7 show the *P*-wave arrival location of the ray with initial declination of 35.5° for each of the models. This indicates the effect the anisotropy can have on the path of a ray, with the ray in model A reaching approximately twice the depth of that for model F.

The difference in travel times for the anisotropic models and those of the isotropic model are shown in Figure 9. The time differences are due to two effects: the different velocities in the salt and the different ray paths. The effects of anisotropy on travel times is significantly larger for the *S*-waves compared to the *P*-waves. The *P*-wave time differences (Fig. 9a) for the most extreme cases reach over 20 ms at depth. For both *S*1-waves (Fig. 9b) and *S*2-waves (Fig. 9c) the most anisotropic model shows time differences with respect to the isotropic model of about 100 ms at a depth of 5 km. The rate of change of the time-differences for the *S*1-waves varies rapidly with depth compared to the *S*2-waves.

The shear-wave splitting for the anisotropic models range from a maximum splitting of 18 ms to one of 58 ms (Fig. 10). After an initial reduction in the magnitude of the splitting in the first kilometre it increases again and stays over 10 ms for all the models to 5 km depth. The amount and sign of the shear-wave splitting will be diagnostic of anisotropy in the salt.

Synthetic seismograms show the effects the variation in anisotropy on the converted waves undergoing conversion at the salt-shale interfaces (Fig. 11). The most noticeable amplitude difference can be seen in the *PSS* ray-group. In the w_{400} = 0.031345 model this ray-group has high amplitude between 1 and 2 km and relatively low elsewhere, this is due to a focusing of rays as seen in Figure 8d. The variation in the other two models is not so extreme. Also note the greater arrival time separation between the *PPS* and *PSP* ray groups

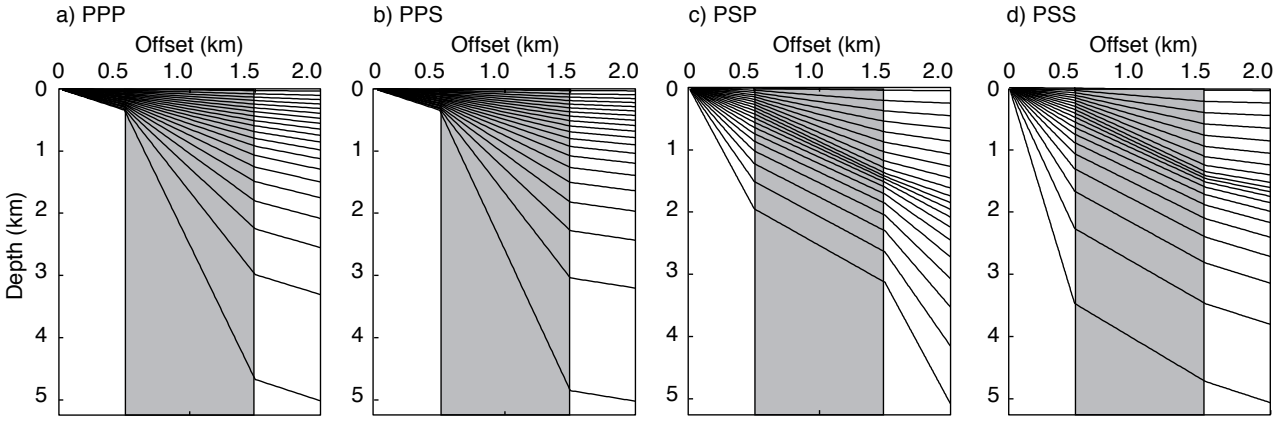

Figure 8

Plots of ray paths for four raygroups in the w_{400} model.
a) *PPP*, *P*-waves throughout raypath;
b) *PPS*, conversion to *S*1-wave on exiting salt;
c) *PSP*, conversion to *S*1-wave on entering salt and conversion back to P-wave on exiting salt;
d) *PSS*, conversion to *S*1-wave on entering salt.

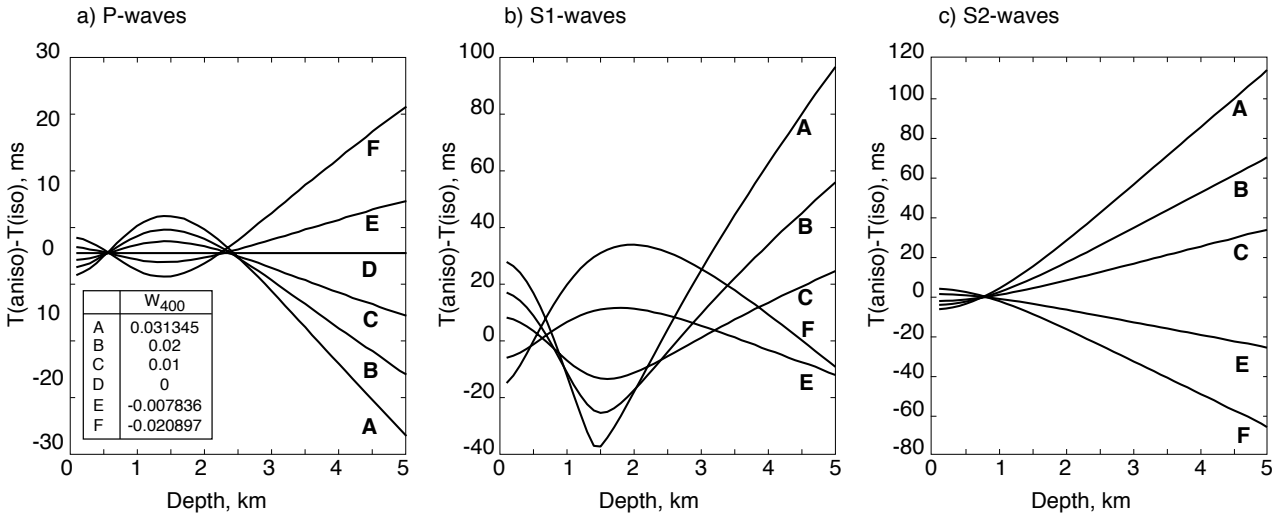

Figure 9

Travel time differences between anisotropic models and those of an isotropic salt model, T(aniso)-T(iso), for:
a) *P*-waves;
b) *S*1-waves;
c) *S*2-waves.

for the w_{400} = –0.020897 model compared to the w_{400} = 0.031345 model.

The difference in travel times between the raygroups in the anisotropic models and isotropic model are shown in Figure 12. The general shape of plot depends upon the wave type in the salt with time differences for *PPS* similar to those of *PPP* and *PSP* similar to those of *PSS* for each model. Up to a depth of 2.5 km the *PPP* and *PPS* raygroups both have low travel time differences. From then they increase continuously until the bottom of the model where, for both models, differences of over 20 ms in magnitude occur. For the *PSP* and *PSS* raygroups the time differences are larger with maximum values in excess of 35 ms. As well as the sign difference between the models there is quite a difference in shape of graph with w_{400} = 0.031345 lines heading towards zero more rapidly at the bottom of the model.

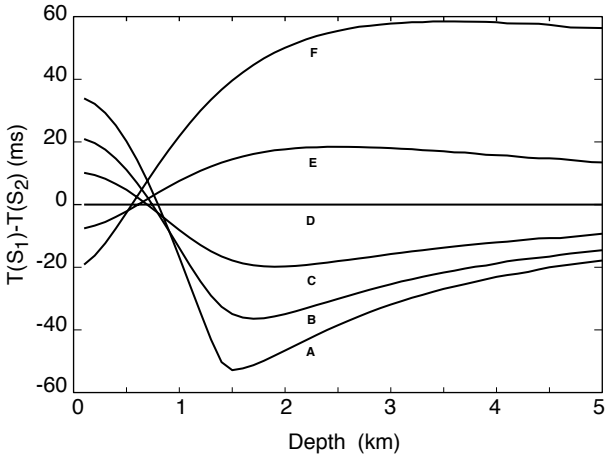

Figure 10

Shear-wave splitting, the travel time difference between the *S*1- and *S*2-waves for each model.

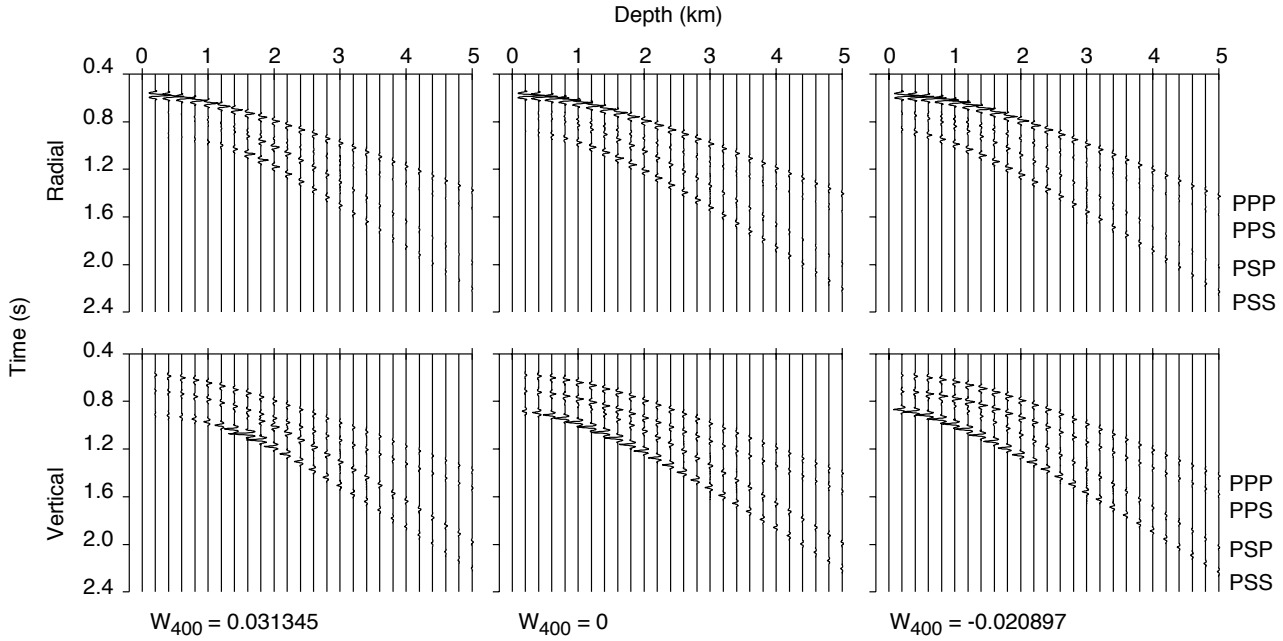

Figure 11

Synthetic seismograms for a *P*-wave undergoing conversions at the salt-shale interfaces. Vertical and radial components are shown for the w_{400} = 0.031345, w_{400} = 0 and w_{400} = -0.020897 models.

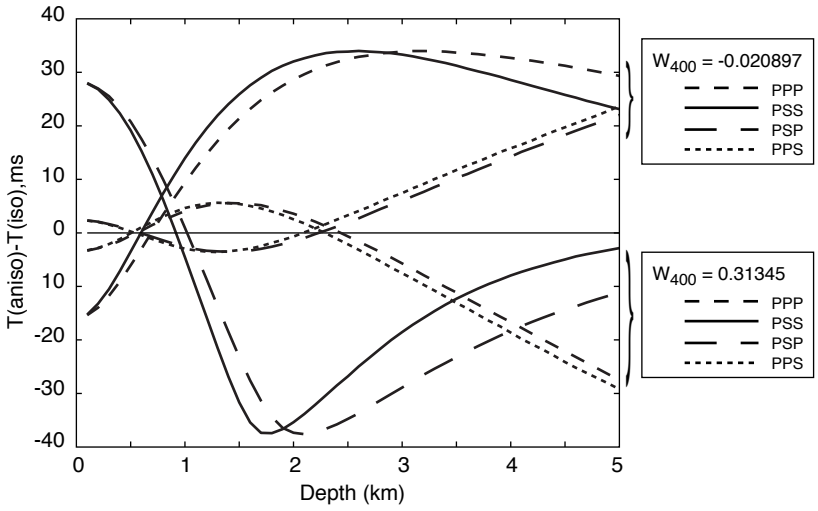

Figure 12

Travel time differences between anisotropic models and those of an isotropic salt model, T(aniso)-T(iso), for the four raygroups, *PPP*, *PPS*, *PSP* and *PSS*.

CONCLUSIONS

The construction and ray-tracing through of seismic models containing anisotropic salt has shown that observable effects on the propagation of seismic waves can occur. Significant travel time differences are observed particularly for shear waves where the difference between anisotropic and isotropic travel times can reach over 100 ms. Anisotropic salt also creates significant shear wave splitting with values of over 50 ms for the most anisotropic cases. This shear wave splitting will be diagnostic of salt anisotropy. Wave conversion is also effected by salt being anisotropic with variation in travel times and amplitudes of the seismic waves.

REFERENCES

Allen A.J., Hutchings M.T., Sayers C.M., Allen D.R. and Smith R.L. (1983) Use of neutron diffraction texture measurements to establish a model for calculation of ultrasonic velocities in highly oriented austenitic weld material. *J. Appl. Phys.*, 54, 555-560.

Carter N.L. and Hansen F.D. (1983) Creep of rocksalt. *Tectonophysics*, 92, 275-333.

Franssen R.C.M.W. and Spiers C.J. (1990) Deformation of polycrystalline salt in compression and in shear at 250-350°C. In: *Deformation Mechanisms, Rheology and Tectonics*, Knipe, R.J. and Rutter, E.H. (Eds.), Geological Society Special Publication, 45, 201-213.

Gebrande H. (1982) in: *Landolt-Börnstein*, N.S. V/1b, Springer-Verlag, 1.

Guest W.S. and Kendall J.M. (1993) Modelling seismic waveforms in anisotropic inhomogeneous media using ray and Maslov asymptotic theory: applications to exploration seismology. *Can. J. Expl. Geophys.*, 29, 78-92.

Jackson M.P.A. Vendeville B.C. and Schultz-Ela D.D. (1994) Structural dynamics of salt systems. *Annu. Rev. Earth Planet. Sci.*, 22 , 93-117.

Jenyon M.K. (1986) *Salt Tectonics*, Elsevier Applied Science.

Kern R. and Richter A. (1985) Microstructures and textures in evaporites. In: *Preferred Orientation in Deformed Metals and Rocks: An Introduction to Modern Texture Analysis*, Wenk H.R. (Ed.), Academic Press, 317-333.

Muehlberger W.R. and Clabaugh P.S. (1968) Internal structure and petrofabrics of Gulf Coast salt domes. In: *Diapirism and Diapirs*, Braunstein J. and O'Brien G.D. (Eds.) *AAPG Memoir*, 8, 90-98.

Roe R.J. (1965) Description of crystallite orientation in polycrystalline materials. III. General solution to pole figure inversion. *J. Appl. Phys.*, 36, 2024-2031.

Roe R.J. (1966) Inversion of pole figures for materials having cubic crystal symmetry. *J. Appl. Phys.*, 37, 2069-2072.

Sayers C.M. (1982) Ultrasonic velocities in anisotropic polycrystalline aggregates. *J. Phys. D.* 15, 2157-2167.

Schwerdtner W.M. (1968) Intergranular gliding in domal salt. *Tectonophysics*, 5, 353-380.

Skrotzki W. and Welch P. (1983) Development of texture and microstructurein extruded ionic polycrystalline aggregates. *Tectonophysics*, 99, 47-61.

Wenk H.R., Canova G., Molinari A. and Mecking H. (1989) Texture development in halite: comparison of Taylor model and self-consistent theory. *Acta Metall.*, 37, 2017-2029.

Final manuscript received in July 1998